CHAPTER

11 Electrical stimulation in a spiking neural network model of monkey superior colliculus

A. John van Opstal[a,*], **Bahadir Kasap**[b]

[a]*Department of Biophysics, Donders Institute for Brain, Cognition and Behaviour, Radboud University Nijmegen, Nijmegen, The Netherlands*

[b]*Department of Biophysics, Radboud University, Donders Centre for Neuroscience, Nijmegen, The Netherlands*

**Corresponding author: Tel.: +31-243-614-251, e-mail address: j.vanopstal@donders.ru.nl*

Abstract

The superior colliculus (SC) generates saccades by recruiting a population of cells in its topographically organized motor map. Supra-threshold electrical stimulation in the SC produces a normometric saccade with little effect of the stimulation parameters. Moreover, the kinematics of electrically evoked saccades strongly resemble natural, visual-evoked saccades. These findings support models in which the saccade vector is determined by a center-of-gravity computation of activated neurons, while trajectory and kinematics arise in brainstem-cerebellar feedback circuits. Recent single-unit recordings, however, have indicated that the SC population also specifies the instantaneous saccade kinematics, supporting an alternative model, in which the saccade trajectory results from dynamic summation of movement effects of all SC spike trains. Here we reconcile the linear summation model with stimulation results, by assuming that the electric field directly activates a relatively small set of neurons around the electrode tip, which subsequently sets up a large population response through lateral synaptic interactions.

Keywords

Saccades, Motor map, Spatial-temporal transformation, Lateral synaptic interactions, Population coding, Vector averaging, Linear summation

1 Introduction

The midbrain superior colliculus (SC) is an important common terminal for cortical and subcortical inputs involved in saccade generation, and specifies a gaze-displacement command for downstream eye-head motor circuitries (Moschovakis et al., 1998; Robinson, 1972; Scudder, 1988). It contains a topographic map of

Progress in Brain Research, Volume 249, ISSN 0079-6123, https://doi.org/10.1016/bs.pbr.2019.04.008

saccade vectors, in which amplitude is represented logarithmically along its rostral-caudal axis, and saccade direction maps roughly linearly along the medial-lateral axis (Ottes et al., 1986; Robinson, 1972).

Each saccade is associated with a translation-invariant Gaussian population, the center of which corresponds to the site of the saccade vector in the map (Ottes et al., 1986; Van Opstal et al., 1990). It is assumed that each recruited neuron encodes a tiny movement contribution, determined by its location in the motor map, and by its activity.

Two competing models have been proposed for decoding this population: weighted averaging of the cells' vector contributions (Lee et al., 1988; Port and Wurtz, 2003; Walton et al., 2005) vs. their linear summation (Goossens and Van Opstal, 2006, 2012; Van Gisbergen et al., 1985):

$$\boldsymbol{S}_{AVG} = \frac{\sum_{n=1}^{N} F_n \bullet \boldsymbol{M}_n}{\sum_{n=1}^{N} F_n} \tag{1a}$$

versus

$$\boldsymbol{S}_{SUM}(t) = \sum_{n=1}^{N} \sum_{k=1}^{K_n<t} \delta(t-\tau_{n,k}) \bullet \boldsymbol{m}_n \tag{1b}$$

N is the number of active neurons in the population, $K_n<t$ is the number of spikes from neuron n up to time t, F_n is mean firing rate, and $\boldsymbol{M}_n$ is the saccade vector encoded at the SC site of cell n; $\boldsymbol{m}_n = \zeta \boldsymbol{M}_n$ is the tiny contribution of cell n in the direction of $\boldsymbol{M}_n$ for each of its spikes (the cell's "*spike vector*"); ζ is a fixed scaling, $\delta(t-\tau_{k,n})$ the k'th spike of neuron n, fired at time $\tau_{k,n}$.

The vector-averaging scheme only specifies the amplitude and direction of the saccade vector, and places the SC motor map outside the kinematic control loop of its trajectory. The nonlinear amplitude-peak velocity relationship of saccades is thus generated by dynamic feedback circuits in brainstem-cerebellar pathways (Jürgens et al., 1981; Lee et al., 1988; Lefèvre et al., 1998; Quaia et al., 1999; Robinson, 1975).

In contrast, the linear spike-vector summation model encodes the full kinematics of the saccade trajectory at the level of the SC motor map through the temporal distribution of all spikes in the population (Goossens and Van Opstal, 2006, 2012). As a result, the instantaneous firing rates of all neurons together encode the saccadic velocity profile.

Clearly, the models of Eqs. (1a) and (1b) cannot both be right. Yet, each is supported by different lines of evidence. For example, micro-stimulation with rectangular current pulse-profiles produces fixed-vector E-saccades with normal kinematics that remain invariant to changing stimulation parameters (Katnani and Gandhi, 2012; Robinson, 1972; Van Opstal et al., 1990; Stanford et al., 1996). The vector-averaging scheme can readily account for this, since the center of gravity of the population only specifies the saccade vector. However, although

the vector-averaging model also predicts the observed pattern of saccadic dysmetrias to focal reversible lesions, it fails to explain the concurrent substantial slowing of saccades (Lee et al., 1988). As this latter observation is accounted for by the linear summation model (Goossens and Van Opstal, 2006), it further supports the idea that the SC population encodes both the saccade-vector and its kinematics.

Micro-stimulation experiments have also shown that at low current strengths, around threshold, E-saccades become smaller and slower than main sequence (Van Opstal et al., 1990; Katnani and Gandhi, 2012). These results do not follow from vector averaging either, but are explained by dynamic summation.

Clearly, if stimulation would produce a population profile that mimics the imposed rectangular current pulse (as is typically assumed), the summation model would generate severely distorted saccade-velocity profiles. Yet, little is known about the actual activity profiles in the motor map during micro-stimulation, as neural recordings during stimulation are not available, or remain obscured by large artifacts.

Two factors determine neuronal activation by micro-stimulation: (1) direct (feed-forward) current stimulation of cell bodies and axons, and (2) synaptic activation through lateral (feedback) connections among the neurons in the motor map. How each factor contributes to the population activity is not known. It is conceivable, however, that the electric field drops rapidly with distance from the electrode tip, so that a relatively small number of neurons would be directly stimulated by the electrode.

Indeed, two-photon imaging in frontal eye fields (FEF) revealed that only a sparse set of neurons was activated directly around the immediate vicinity of the stimulation site (Histed et al., 2009), suggesting that the major factor may be synaptic transmission.

We recently constructed a spiking neural network model with lateral interactions in the SC that explains the single-unit activity patterns around saccades (Kasap and Van Opstal, 2017). It accounts for the observed firing rates of collicular cells (Goossens and Van Opstal, 2006, 2012) in response to neural input from upstream sources (e.g., FEF). This paper provides a brief overview on how the model might cope with the effects of electrical micro-stimulation (see Kasap and Van Opstal, 2019, for a full account).

2 Methods and results

2.1 Afferent mapping

The afferent mapping function maps the target (R, ϕ), in visual space, to the anatomical coordinates, (u,v) (in mm), of the SC motor map (Ottes et al., 1986). We here simplified this mapping by the complex logarithm:

$$u(R) = B_u \cdot \ln(R) \text{ and } v(\phi) = B_v \cdot \phi \quad (2)$$

with $B_u = 1.0$ mm and $B_v = 1.0$ mm/rad (isotropic map). Thus, the infinitesimal movement contribution, $\boldsymbol{m} = (m_x, m_y)$, of a single spike at site (u,v) to the eye movement (Eq. 1b) is given by the scaled efferent mapping:

$$m_x = \zeta \cdot \exp(u) \cdot \cos(v) \text{ and } m_y = \zeta \cdot \exp(u) \cdot \sin(v) \tag{3}$$

2.2 Network characteristics

We constructed a 2D spiking neural network model as a rectangular grid of 201×201 neurons (e.g., Fig. 3A), and simulated the network dynamics in C++/CUDA (Nickolls et al., 2008). In the simulations we employed dynamic parallelism to accelerate spike propagation on a GPU (Kasap and Van Opstal, 2018).

Neurons were modeled as adaptive exponential integrate-and-fire (AdEx; Brette and Gerstner, 2005), which reduces the Hodgkin-Huxley equations to two state variables: membrane potential, $V(t)$, and adaptation current, $q(t)$. The neuronal dynamics are determined by two coupled, nonlinear differential equations and a spiking-reset (Fig. 1B). For neuron n:

$$C\frac{dV_n}{dt} = -g_L(V_n - E_L) + g_L\eta \exp\left(\frac{V_n - V_T}{\eta}\right) - q_n + I_{inp,n}(t) \tag{4a}$$

$$\tau_{q,n}\frac{dq_n}{dt} = a(V_n - E_L) - q_n \tag{4b}$$

$$\text{at } t = \tau_{\text{spk}} : V(\tau_{\text{spk}}) \rightarrow V_{rst} \text{ and } q(\tau_{\text{spk}}) \rightarrow q(\tau_{\text{spk}}) + b \tag{4c}$$

with C the membrane capacitance, g_L the leak conductance, E_L the leak reversal potential, η a slope, V_T the neural spiking threshold, V_{rst} the reset potential, $\tau_{q,n}$ the adaptation time constant, and a the sub-threshold adaptation constant. Fig. 1C shows the response patterns of three AdEx neurons to different input currents and membrane properties.

In Eq. (4a), $I_{inp,n}$ is the neuron's total synaptic input current, provided by the lateral interactions with other neurons, and the externally applied micro-stimulation current (Fig. 1A):

$$I_{inp,n}(t) = g_n^{exc}(t)(E_e - V_n(t)) + g_n^{inh}(t)(E_i - V_n(t)) + I_E(u_n, v_n, t) \tag{5}$$

The lateral synaptic connections of neuron n with other neurons in the map are described by a Mexican-hat profile (Trappenberg et al., 2001), with local (σ_{exc}) excitatory and global (σ_{inh}) inhibitory projections ($\sigma_{\text{exc}} > \sigma_{\text{exc}}$; Fig. 2B). This profile has an overall synaptic scaling factor, s_n, depending on a cell's location (Fig. 2A). Neurons thus underwent strong short-range excitatory and weak long-range inhibitory influences through a dynamic soft winner-take-all mechanism. The "winner" governs the activity patterns of all other active neurons, inducing spike-train synchronization in the population (Goossens and Van Opstal, 2012; Kasap and Van Opstal, 2017; Fig. 2C).

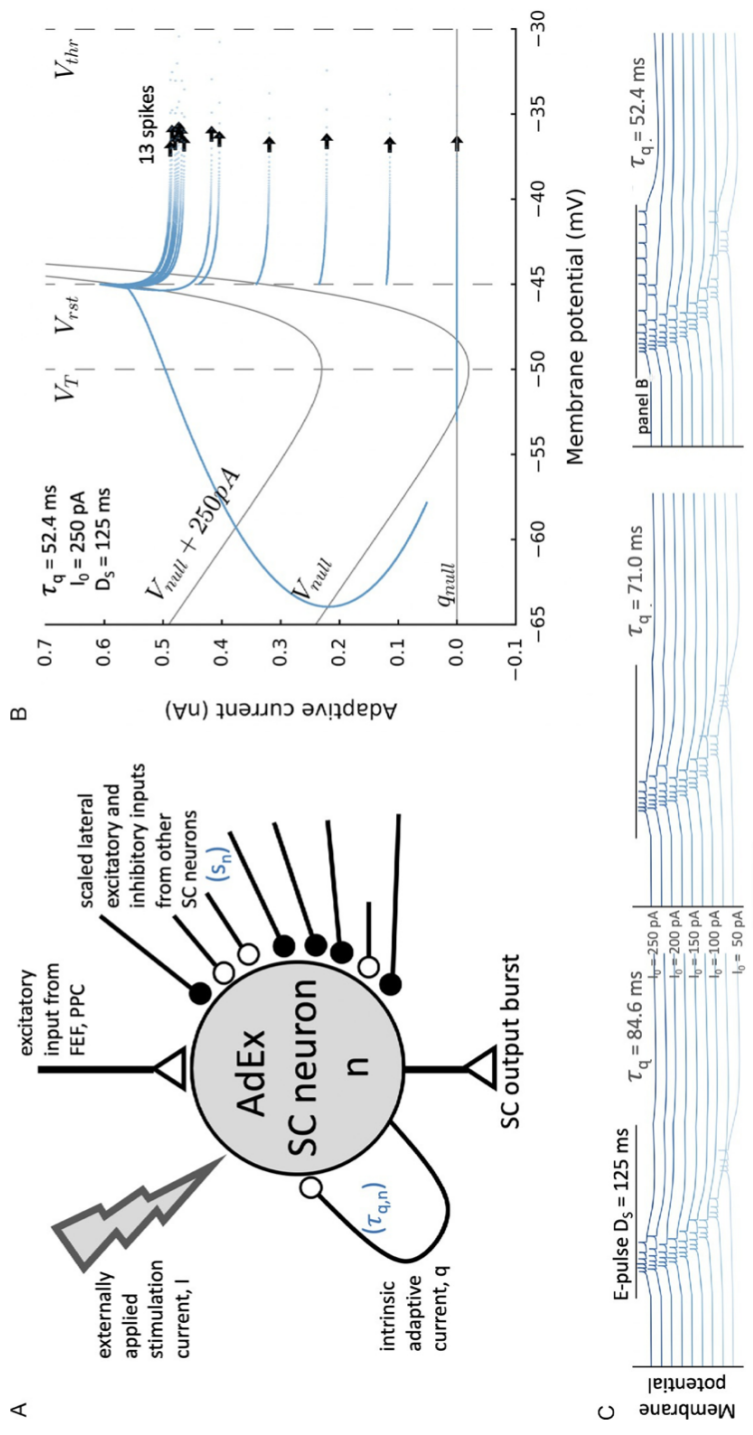

FIG. 1

(A) Schematic representation of an AdEx spiking SC neuron; two tuning parameters, s_n and $\tau_{q,n}$ determine its spiking behavior. (B) Phase plot (membrane potential vs. adaptive current) of the neuronal response (with τ_q = 52.4 ms) to micro-stimulation (I_0 = 250 pA, D_S = 125 ms). V- and q-nullclines are fixed-point trajectories of Eq. (4a) and (4b). Spike occurrences are indicated by arrows. (C) Responses of three model neurons (τ_q = 84.6 ms, τ_q = 70.95 ms, and τ_q = 52.4 ms) to micro-stimulation at different current strengths (colored traces; D_S = 125 ms).

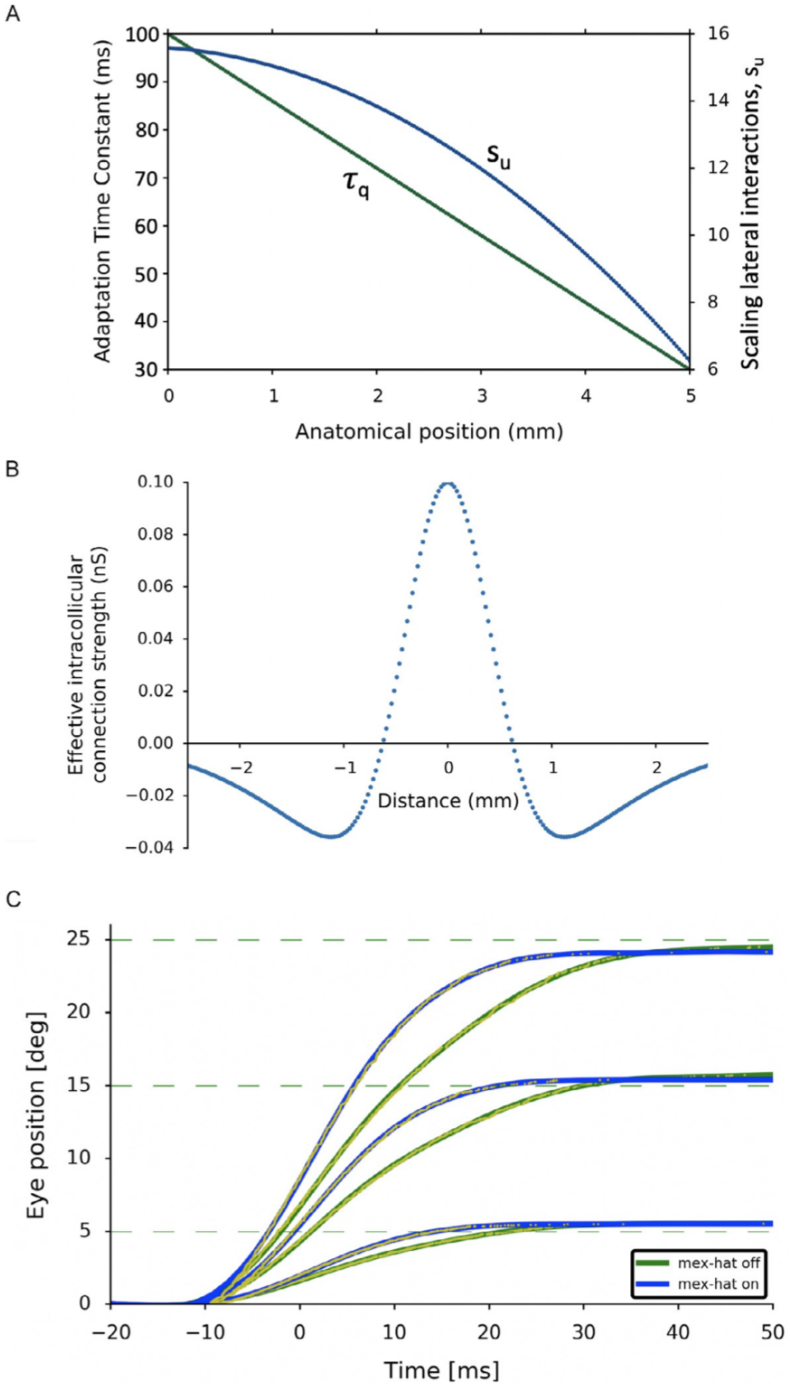

FIG. 2

(A) Result of tuning the site-dependent parameters in the model: $\tau_{q,n}$ (green line) and s_n (blue line), as function of u. (B) Lateral-interaction profile in the network, for a neuron in the center of the motor map. (C) Result of simulated saccades for two situations: without lateral interactions (green) and with lateral interactions (blue). The latter saccades are considerably faster, because of synchronization of neural activity in the population with the most-active neuron (see Fig. 3B).

2.3 Current spread

We applied electrical stimulation with an external current, centered around $[u_E, v_E]$, with an exponential spatial decay of the effective electric field:

$$I_E(u,v,t) = I_0 \cdot \exp\left(-\lambda \cdot \sqrt{(u-u_E)^2 + (v-v_E)^2}\right) \cdot P(t) \quad (6)$$

with λ (mm^{-1}) the spatial decay constant, I_0 the current intensity (in pA), and a rectangular stimulation pulse, $P(t)$, with duration D_S.

2.4 Network tuning

Intrinsic biophysical properties of the neurons were enforced by systematically varying the adaptation time constant, $\tau_{q,n}$, and the synaptic weight-scaling parameter, s_n. By tuning these two parameters, we accounted for the systematically changing firing properties of SC cells along the rostral-caudal axis of the motor map, while keeping a fixed number of spikes for the neurons' preferred saccades across the map. We used a genetic algorithm to find appropriate location-dependent $[\tau_{q,n}, s_n]$ pairs for the neurons, to ensure a fixed number of spikes per neuron under a given micro-stimulation condition, and the subsequent excitation profile through the lateral interactions (Fig. 3A). All parameters are summarized in Appendix.

2.5 Micro-stimulation

Fig. 3A–C shows the effect of micro-stimulation at a caudal location in the motor map, yielding an oblique saccade with an amplitude of 31 deg. The size of the resulting population is very similar to that of a visual stimulus ($\sigma_{POP} = 0.5$ mm; Kasap and Van Opstal, 2017), and also the number of spikes elicited by the cells ($N = 20$ for the central cell, see color bar) corresponds to the normal condition. The peak firing rates of the neurons reached a maximum of about 450 spikes/s, with burst durations up to about 70 ms. The saccade reached a peak velocity of ~900 deg/s, while horizontal and vertical velocity profiles have identical shapes, indicating a straight oblique trajectory.

2.6 Kinematics

Fig. 4A and B presents E-saccades for nine stimulation sites along the horizontal meridian. Note that saccade duration increases with saccade amplitude, and that peak eye velocity shows a less than linear increase with saccade size. The nonlinear, saturating main sequence of these E-saccades is shown in Fig. 4C. We also verified that the saccades remained invariant to a wide range of stimulation parameters, which is illustrated in Fig. 4D. Around the threshold (around 80 pA), the peak velocity decreased substantially, but without affecting E-saccade amplitudes (not shown).

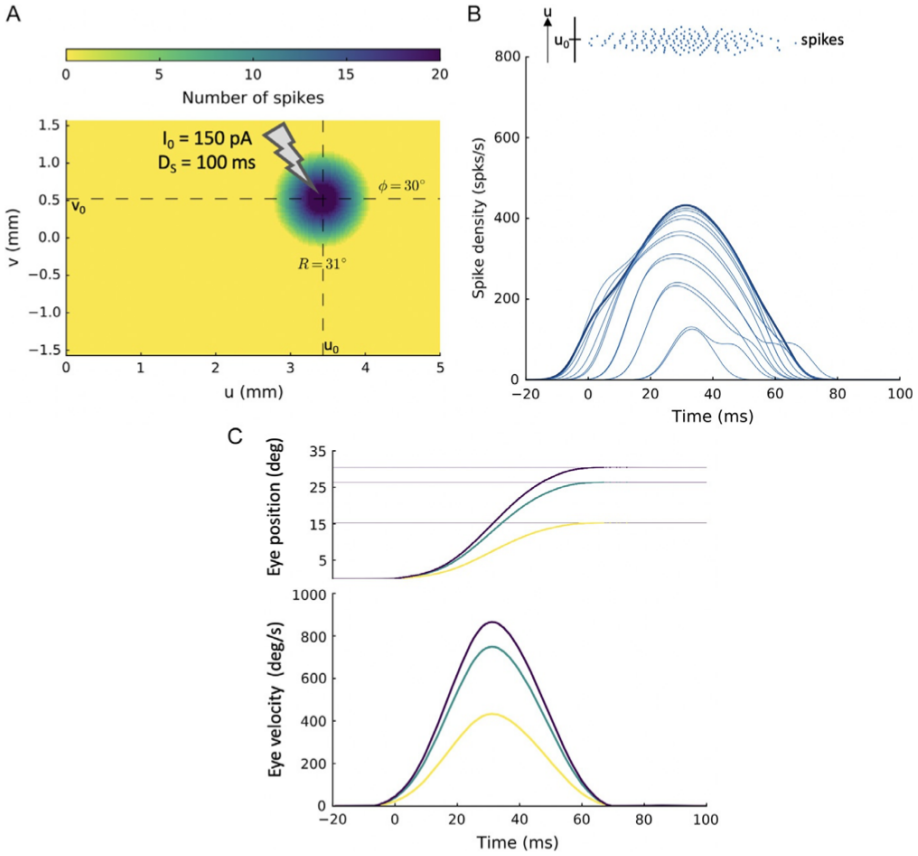

FIG. 3

(A) Spike counts in the motor map from the recruited population to micro-stimulation at $(u_E,v_E)=(3.2,0.5)$ mm. (B) Burst profiles of the model neurons (at 0.1 mm intervals from the central cell along the u-direction) portray synchronized population activity. (C) Eye displacement and eye velocity from linear dynamic ensemble-coding (Eq. 1b; horizontal (green), vertical (yellow), and vectorial (purple) traces).

3 Discussion

The linear ensemble-coding model of Eq. (1b) (Goossens and Van Opstal, 2006; Van Gisbergen et al., 1987; Van Opstal and Goossens, 2008) is inconsistent with micro-stimulation results, when it is assumed that (i) a rectangular stimulation input profile (Eq. 6) directly imposes the firing patterns on the neural population, and (ii) neurons are independent, without synaptic interactions.

We here argued that these assumptions are neither supported by experimental observations, nor do they incorporate the possibility that a major factor determining the recruitment of SC neurons is caused by synaptic transmission within the motor map, rather than by direct activation through the electrode's electric field. We

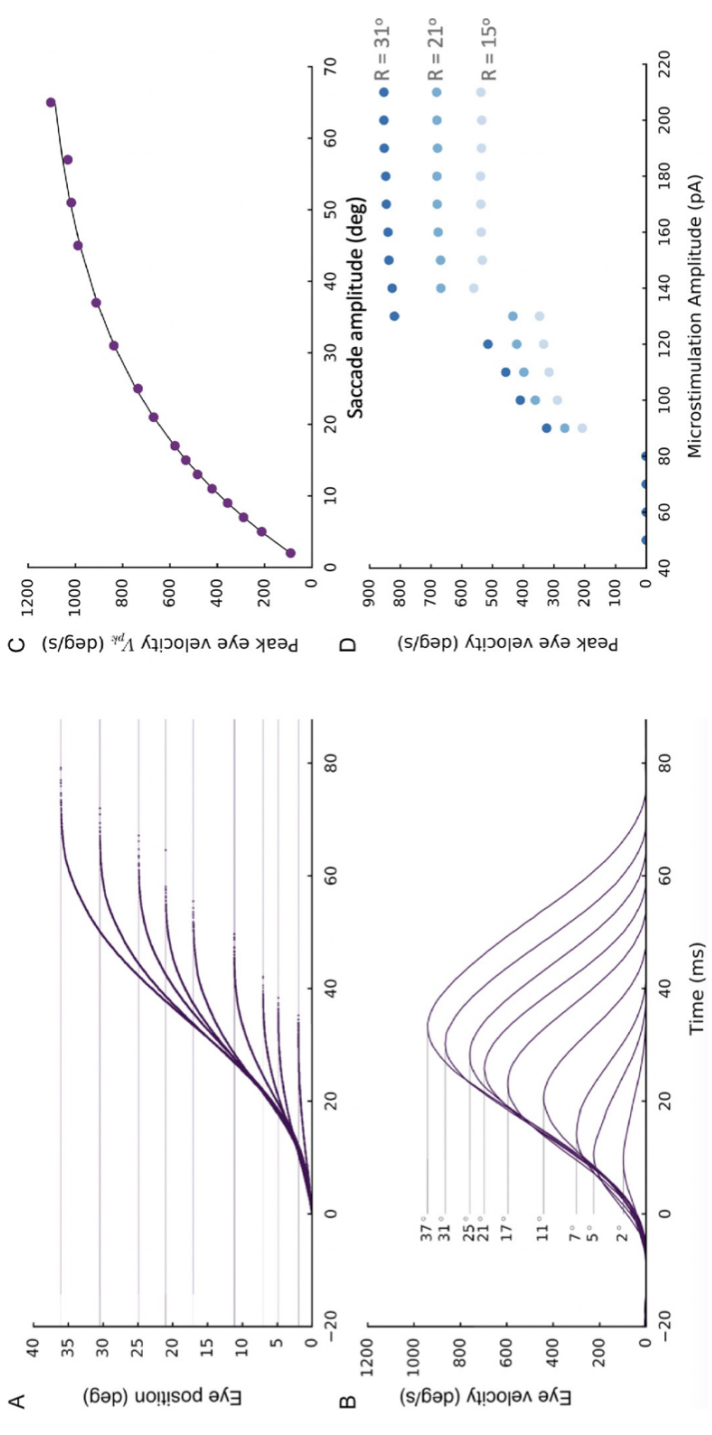

FIG. 4

(A) Eye-displacement traces for nine horizontal E-saccades, elicited with $I_0 = 150$ pA, $D_S = 100$ ms at different sites in the motor map. (B) Eye-velocity profiles for the position traces in A. Note the clear increase in saccade duration, and the sublinear increase of peak eye-velocity with saccade amplitude. (C) A nonlinear, saturating main sequence, despite fully linear weighting of SC spike vectors (Eq. 1b). (D) Above 125 pA, saccade kinematics remained invariant for a large range of stimulation strengths. Near threshold (~80 pA), they became markedly slower.

implemented circular-symmetric, Mexican-hat like interactions in a spiking neural network model of the SC motor map and assumed that the current profile from the electrode rapidly decreased with distance from the electrode tip. As a consequence, only neurons in the direct vicinity (<0.1 mm) of the electrode were activated by the external electric field (Histed et al., 2009), insufficient to generate the saccade according to spike-vector summation (Eq. 1b).

Once neurons were recruited by the stimulation pulse, however, local excitatory synaptic transmission among nearby cells rapidly spread the activation to create a neural activity pattern which, within 10–15 ms, was dictated by the bursting dynamics of the most active central cells in the population (Fig. 3B, top). As a result, all cells synchronized their peak firing rates, and burst shapes within the population were highly correlated. Similar response properties have been reported in recordings for natural, sensory-evoked saccades (Goossens and Van Opstal, 2012). According to the dynamic spike-summation model (Eq. 1b), such high level of neuronal synchronization ensures an optimally strong input to the brainstem saccadic burst generator to accelerate the eye with the maximally possible innervation.

3.1 Network tuning

The lateral excitatory-inhibitory synaptic interactions, in combination with the site-dependent tuning of the neurons' biophysical parameters (Fig. 2A), ensured three important aspects of collicular firing patterns observed during saccade execution: (i) they set up a large, but limited, population of cells, invariant across the SC motor map, in which the total activity (quantified by the number of spikes elicited by the recruited cells) can be described by a circular-symmetric Gaussian with a width (standard deviation) of approximately 0.5 mm, (ii) the temporal firing patterns of the central cells (their peak firing rate, burst shape, and burst duration) depend uniquely on their location in the motor map, while the number of spikes in the burst remains invariant across the map, and for a wide range of micro-stimulation parameters, and (iii) already within the first couple of spikes, the recruited neurons all became synchronized throughout the population, in which the most active cells (those in the center) determined the spike-density profiles of all the others.

3.2 Network normalization

Only close to stimulation threshold, the evoked activity remained much lower than for supra-threshold stimulation currents, leading to excessively slow eye movements (Fig. 4D), starting at a longer latency. Similar results have been reported for micro-stimulation experiments (e.g., Katnani and Gandhi, 2012; Van Opstal et al., 1990). The peak eye-velocity of our model saccades followed a psychometric curve as function of the applied current strength (Fig. 4D), whereas the kinematics of eye movements evoked near-threshold became much slower than main sequence. This property is readily predicted by the linear spike-vector summation model (Eq. 1b), but does not follow from center-of-gravity computational schemes (like Eq. 1a), in which the activity patterns themselves are immaterial for evoked saccade kinematics.

Conceptually, the lateral interactions serve to normalize the population activity, and to synchronize neural activity across cells. As a result, the total number of spikes emanating from the SC population is constant across the motor map for a large range of (sensory or electrical) stimulation parameters. The nonlinear normalization of Eq. (1b) is thus automatically implemented through the intrinsic organization of the SC network dynamics, and does not require an additional downstream "spike-counting" mechanism to terminate the saccade, as suggested earlier by Van Opstal and Goossens (2008) (but see, e.g., Van Opstal and Van Gisbergen, 1989a).

Although other network architectures, relying, e.g., on presynaptic inhibition across the dendritic tree, can accomplish normalization of the population and implement vector averaging (Carandini and Heeger, 1994; Groh, 2001; Van Opstal and Goossens, 2008; Van Opstal and Van Gisbergen, 1989a,b), anatomical evidence to support such nonlinear mechanisms is lacking. We here showed that simple linear summation of the effective synaptic inputs at the cell's membrane, which is a well-recognized physiological mechanism of basic neuronal functioning, can implement such normalization when it is combined with excitatory-inhibitory communication among the neurons within the same, topographically organized structure. Such a simple mechanism could suffice to ensure (nearly) invariant gaze-motor commands across a wide range of competing neuronal inputs.

3.3 In conclusion

The spatial dependence of the lateral excitatory-inhibitory synaptic interactions and the adaptation time constants of collicular neurons in the collicular motor map (Fig. 2A), betrays a neural organization that aims to optimize speed-accuracy trade-off for saccades (Harris and Wolpert, 2006). As emerging properties of our linear model, cells in the neural population synchronize their bursts to provide a maximally effective pulse to the brainstem saccadic circuitry (Goossens and Van Opstal, 2012), and oblique saccades follow straight trajectories with saccade-component cross-coupling (Smit et al., 1990). Because of the simple linear population read-out (spike-vector summation), there is no need for either a nonlinear weighting mechanism of the SC population, like vector averaging (Walton et al., 2005), a non-linear threshold mechanism in a putative downstream spike counter (Goossens and Van Opstal, 2006), or presynaptic inhibition (Carandini and Heeger, 1994; Groh, 2001). Furthermore, because in the model the saccade kinematics are encoded by the spatial gradient in the SC motor map, the nonlinear saturating burst generators in the brainstem (Harris and Wolpert, 2006; Jürgens et al., 1981; Van Gisbergen et al., 1981) may, in fact, operate as linear component pulse generators.

We here investigated the neural population dynamics, by assuming that micro-stimulation merely provides direct electrical input to a small group of cells near the electrode. Due to the lateral interactions, the population rapidly grows to an activity profile that is virtually indistinguishable from the visual-evoked condition. As described in our companying paper (Van Opstal and Kasap, 2019; this volume), this simple organization may be readily extended to the full eye-head gaze-control system.

Acknowledgments

This work was supported by the European Commission through a Horizon 2020 ERC Advanced Grant, project ORIENT (grant 693400; A.J.v.O.; B.K.). The Tesla K40 used for this research was donated by the NVIDIA Corporation.

Appendix: Parameter values used in the simulations

Micro-stimulation parameters		
λ	**10 mm^{-1}**	**Spatial decay constant**
I_0	150 (40–280) pA	Intracellular current intensity
$P(t)$	I_0 (for $0<t<D_s$)	Rectangular stimulus pulse
D_S	100 (25–250) ms	Stimulation duration
Neural parameters		
C	600 pF	Membrane capacitance
g_L	20 nS	Leak conductance
E_L	−53 mV	Leak reversal potential
η	2 mV	Spike slope factor
V_T	−50 mV	Exponential threshold
V_{peak}	−30 mV	Spiking threshold
V_{rst}	−45 mV	Reset potential
a	0 nS	Sub-threshold adaptation
b	120 pA	Spike-triggered adaptation
$\tau_{q,n}$	100–30 ms	Location-dependent adaptation time constant; varies with (u_n), see Fig. 2A.
ζ	$5.087 \cdot 10^{-5}$	Efferent map mini-vector scaling factor
Synaptic parameters		
E_{exc}	0 mV	Excitatory reversal potential
E_{inh}	−80 mV	Inhibitory reversal potential
τ_{exc}	5 ms	Excitatory conductance decay
τ_{inh}	10 ms	Inhibitory conductance decay
Lateral connectivity parameters		
$\overline{w}_{exc}$	45 pS	Fixed excitatory scaling factor
σ_{exc}	0.4 mm	Range of excitatory synapses
$\overline{w}_{inh}$	14 pS	Fixed inhibitory scaling factor
σ_{inh}	1.2 mm	Range of inhibitory synapses
s_n	0.0112–0.0147	Location-dependent synaptic scaling factor; varies with (u_n), see Fig. 2A.

References

Brette, R., Gerstner, W., 2005. Adaptive exponential integrate-and-fire model as an effective description of neuronal activity. J. Neurophysiol. 94, 3637–3642.

Carandini, M., Heeger, D.J., 1994. Summation and division by neurons in primate visual cortex. Science 264, 1333–1336.

Goossens, H.H.L.M., Van Opstal, A.J., 2006. Dynamic ensemble coding of saccades in the monkey superior colliculus. J. Neurophysiol. 95, 2326–2341.

Goossens, H.H.L.M., Van Opstal, A.J., 2012. Optimal control of saccades by spatial-temporal-activity patterns in monkey superior colliculus. PLoS Comput. Biol. 8 (5),e1002508.

Groh, J.M., 2001. Converting neural signals from place codes to rate codes. Biol. Cybern. 85, 159–165.

Harris, C.M., Wolpert, D.M., 2006. The main sequence of saccades optimizes speed-accuracy trade-off. Biol. Cybern. 95, 21–29.

Histed, M.H., Bonin, V., Reid, R.C., 2009. Direct activation of sparse, distributed populations of cortical neurons by electrical microstimulation. Neuron 63, 508–522.

Jürgens, R., Becker, W., Kornhuber, H., 1981. Natural and drug-induced variations of velocity and duration of human saccadic eye movements: evidence for a control of the neural pulse generator by local feedback. Biol. Cybern. 96, 87–96.

Kasap, B., Van Opstal, A.J., 2017. A spiking neural network model of the midbrain superior colliculus that generates saccadic motor commands. Biol. Cybern. 111, 249–268.

Kasap, B., Van Opstal, A.J., 2018. Dynamic parallelism for synaptic updating in GPU-accelerated spiking neural network simulations. Neurocomputing 302, 55–65.

Kasap, B., Van Opstal, A.J., 2019. Micro-stimulation in a spiking neural network model of the midbrain superior colliculus. PLoS Comput. Biol. 15 (4), e1006522. https://doi.org/10.1371/journal.pcbi.1006522.

Katnani, H.A., Gandhi, N.J., 2012. The relative impact of microstimulation parameters on movement generation. J. Neurophysiol. 108, 528–538.

Lee, C., Rohrer, W.H., Sparks, D.L., 1988. Population coding of saccadic eye movements by neurons in the superior colliculus. Nature 332, 357–360.

Lefèvre, P., Quaia, C., Optican, L.M., 1998. Distributed model of control of saccades by superior colliculus and cerebellum. Neural Netw. 11, 1175–1190.

Moschovakis, A.K., Kitama, T., Dalezios, Y., Petit, J., Brandi, A.M., Grantyn, A.A., 1998. An anatomical substrate for the spatiotemporal transformation. J. Neurosci. 18, 10219–10229.

Nickolls, J., Buck, I., Garland, M., Skadron, K., 2008. Scalable parallel programming with CUDA. AMC Queue 6, 40–53.

Ottes, F.P., Van Gisbergen, J.A.M., Eggermont, J.J., 1986. Visuomotor fields of the superior colliculus: a quantitative model. Vis. Res. 26, 857–873.

Port, N.L., Wurtz, R.H., 2003. Sequential activity of simultaneously recorded neurons in the superior colliculus during curved saccades. J. Neurophysiol. 90, 1887–1903.

Quaia, C., Lefèvre, P., Optican, L.M., 1999. Model of the control of saccades by superior colliculus and cerebellum. J. Neurophysiol. 82, 999–1018.

Robinson, D.A., 1972. Eye movements evoked by collicular stimulation in the alert monkey. Vis. Res. 12, 1795–1808.

Robinson, D.A., 1975. Oculomotor control signals. In: Lennerstrand, G., Bach-Y-Rita, P. (Eds.), Basic Mechanisms of Ocular Motility and their Clinical Implications. Pergamon Press, pp. 337–374.

Scudder, A., 1988. A new local feedback model of the saccadic burst generator. J. Neurophysiol. 59, 1455–1475.

Smit, A.C., Van Opstal, A.J., Van Gisbergen, J.A.M., 1990. Component stretching in fast and slow oblique saccades in the human. Exp. Brain Res. 81, 325–334.

Stanford, T.R., Freedman, E.G., Sparks, D.L., 1996. Site and parameters of microstimulation: evidence for independent effects on the properties of saccades evoked from the primate superior colliculus. J. Neurophysiol. 76, 3360–3381.

Trappenberg, T.P., Dorris, M.C., Munoz, D.P., Klein, R.M., 2001. A model of saccade initiation based on the competitive integration of exogenous and endogenous signals in the Superior Colliculus. J. Cogn. Neurosci. 13, 256–271.

Van Gisbergen, J.A.M., Robinson, D.A., Gielen, S., 1981. A quantitative analysis of generation of saccadic eye movements by burst neurons. J. Neurophysiol. 45, 417–442.

Van Gisbergen, J.A.M., Van Opstal, A.J., Schoenmakers, J.J.M., 1985. Experimental test of two models for the generation of oblique saccades. Exp. Brain Res. 57, 321–336.

Van Gisbergen, J.A.M., Van Opstal, A.J., Tax, A.A.M., 1987. Collicular ensemble coding of saccades based on vector summation. Neuroscience 21, 541–555.

Van Opstal, A.J., Goossens, H.H.L.M., 2008. Linear ensemble coding in midbrain superior colliculus specifies the saccade kinematics. Biol. Cybern. 98, 561–577.

Van Opstal, A.J., Kasap, B., 2019. Maps and sensorimotor transformations for eye-head gaze shifts: role of the midbrain superior colliculus. In: Mathematical Modeling in Motor Neuroscience: State of the Art and Translation to the Clinic. Progress in Brain Research. vol. 248. Elsevier.

Van Opstal, A.J., Van Gisbergen, J.A.M., 1989a. A nonlinear model for collicular spatial interactions underlying the metrical properties of electrically elicited saccades. Biol. Cybern. 60, 171–183.

Van Opstal, A.J., Van Gisbergen, J.A.M., 1989b. A model for collicular efferent mechanisms underlying the generation of saccades. Brain Behav. Evol. 33, 90–94.

Van Opstal, A.J., Van Gisbergen, J.A.M., Smit, A.C., 1990. Comparison of saccades evoked by visual stimulation and collicular electrical stimulation in the alert monkey. Exp. Brain Res. 79, 299–312.

Walton, M.M.G., Sparks, D.L., Gandhi, N.J., 2005. Simulations of saccade curvature by models that place superior colliculus upstream from the local feedback loop. J. Neurophysiol. 93, 2354–2358.

Further reading

Georgopoulos, A.P., Schwartz, A.B., Kettner, R.E., 1986. Neuronal population coding of movement direction. Science 233, 1416–1419.

Katnani, H.A., Van Opstal, A.J., Gandhi, N.J., 2012. A test of spatial-temporal decoding mechanisms in the superior colliculus. J. Neurophysiol. 107, 2442–2452.

Van Opstal, A.J., 2016. The Auditory System and Human Sound Localization Behavior. Elsevier Publishers, Academic Press, Amsterdam.

Van Opstal, A.J., Van Gisbergen, J.A.M., 1987. Skewness of saccadic velocity profiles: a unifying parameter for normal and slow saccades. Vis. Res. 27, 731–745.